



HAL
open science

A resilience-based framework for the optimal coupling of interdependent critical infrastructures

Andrea Bellè, Adam Abdin, Zhiguo Zeng, Yi-Ping Fang, Anne Barros

► To cite this version:

Andrea Bellè, Adam Abdin, Zhiguo Zeng, Yi-Ping Fang, Anne Barros. A resilience-based framework for the optimal coupling of interdependent critical infrastructures. 2022. hal-03446712v3

HAL Id: hal-03446712

<https://hal.science/hal-03446712v3>

Preprint submitted on 11 Jul 2022

HAL is a multi-disciplinary open access archive for the deposit and dissemination of scientific research documents, whether they are published or not. The documents may come from teaching and research institutions in France or abroad, or from public or private research centers.

L'archive ouverte pluridisciplinaire **HAL**, est destinée au dépôt et à la diffusion de documents scientifiques de niveau recherche, publiés ou non, émanant des établissements d'enseignement et de recherche français ou étrangers, des laboratoires publics ou privés.

A resilience-based framework for the optimal coupling of interdependent critical infrastructures

Andrea Bellè^{1*}, Adam F. Abdin², Zhiguo Zeng¹, Yi-Ping Fang¹, Anne Barros¹

¹*Chair on Risk and Resilience of Complex Systems, Laboratoire Génie Industriel, CentraleSupélec, Université Paris-Saclay, 3 Rue Joliot Curie, 91190 Gif-sur-Yvette, France.*

Emails: andrea.belle@centralesupelec.fr, zhiguo.zeng@centralesupelec.fr, yiping.fang@centralesupelec.fr, anne.barros@centralesupelec.fr

²*Laboratoire Génie Industriel, CentraleSupélec, Université Paris-Saclay, 3 Rue Joliot Curie, 91190 Gif-sur-Yvette, France.*

Email: adam.abdin@centralesupelec.fr

Abstract

As critical infrastructures (CIs) are essential for the safety and socio-economic stability of a society, ensuring their resilience is a task of the utmost importance. Critical infrastructures are often interdependent on each other, and the topology of the interdependencies between different systems, also referred to as coupling interface, plays a key role in terms of their resilience against failures. In case of failures due to natural events, random disturbances, or deliberate attacks, the design of the coupling interface is a key factor for maintaining high performance within the interdependent CIs. However, in the existing literature, the issue of the coupling interface design is often addressed through heuristics. In this work, we propose an optimization-based mathematical approach for designing coupling interfaces between interdependent critical infrastructures under random failures. The proposed approach allows designing a coupling interface that is robust against the worst realization of a set of feasible failure scenarios. Using as case-study interdependent power and gas networks, we show that the proposed method outperforms existing solutions based on network metrics-based heuristics.

Keywords: Coupling interface, resilience, defender-attacker-defender, interdependent critical infrastructures, optimization

List of Symbols

Abbreviations

CI Critical infrastructure

*Corresponding author

Email address: andrea.belle@centralesupelec.fr (Andrea Bellè¹)

GN Gas network

IPGNs Interdependent power and gas networks

NC&CG Nested Column&Constraint Generation

PN Power network

Sets

E_{GN} Set of edges in the gas network

E_{PN} Set of edges in the power network

V_{GN} Set of nodes in the gas network

V_{PN} Set of nodes in the power network

Parameters and coefficients

$\bar{\theta}$ Maximum value of phase angle

\bar{d}_i^b Base requested power demand of node i in the power or gas network

$\bar{d}_j^{m^3}$ Requested gas demand of node j in the gas network

\bar{d}_j^{MW} Requested power demand of node j in the gas network

\bar{d}_{GN} Total requested gas demand of the gas network

\bar{d}_{PN} Total requested power demand of the power network

\bar{f}_k Flow capacity of edge k in the power or gas network

\bar{p}_i Production capacity of node i in the power or gas network

K_{att} Maximum number of attacked edges

L_{GN} Number of edges in the gas network

L_{PN} Number of edges in the power network

M_k Big-M method constant

N_{GN} Number of nodes in the gas network

N_{PN} Number of nodes in the power network

w_{GN} Weight of the gas network

w_{PN} Weight of the power network
 x_k Reactance of edge k in the power network

Variables

δ_j^g Binary variable that indicates the functional state of all the interdependency links starting from node j in the gas network
 δ_j^p Binary variable that indicates the functional state of all the interdependency links starting from node j in the power network
 η Variable of outer layer of NC&CG algorithm
 ρ Variable of inner layer of NC&CG algorithm
 θ_i Phase angle of node i in the power network
 d_i Supplied demand in node i in the power or gas network
 f_k Flow in edge k in the power or gas network
 p_i Production in node i in the power or gas network
 u_k Binary variable that indicates the functional state of edge k in the power network
 $y_{ij}^{g \leftarrow p}$ Binary variable that indicates if a physical link from node $j \in V_{PN}$ to node $i \in V_{GN}$ exists
 $y_{ij}^{p \leftarrow g}$ Binary variable that indicates if a physical link from node $j \in V_{GN}$ to node $i \in V_{PN}$ exists

1. Introduction

1.1. Motivation

Critical infrastructures (CIs), such as power networks or transportation systems, are complex systems which supply goods, services, and commodities to people [1], [2]. Failures and disruption within CIs can lead to severe socioeconomic stress in a society [3], and ensuring their resilience against a large variety of disruptive events is an important issue [4], [5]. Moreover, CIs are increasingly interdependent on each other. This increasing degree of interdependency brings advantages in terms of functionality and efficiency, but often leads to new vulnerabilities and risks of cascading effect between interdependent infrastructures [6].

Coupling interfaces play a key role in characterizing the resilience of interdependent CIs [7], [8]. The coupling interface characterizes how the interdependent CIs are coupled together; in other words, it characterizes how the interdependent CIs are connected and what are the components in

each CI that are dependent on the other CI. When CIs are modeled as networks [9], the coupling interface simply denotes the allocation of interdependency links, as shown in Figure 1.

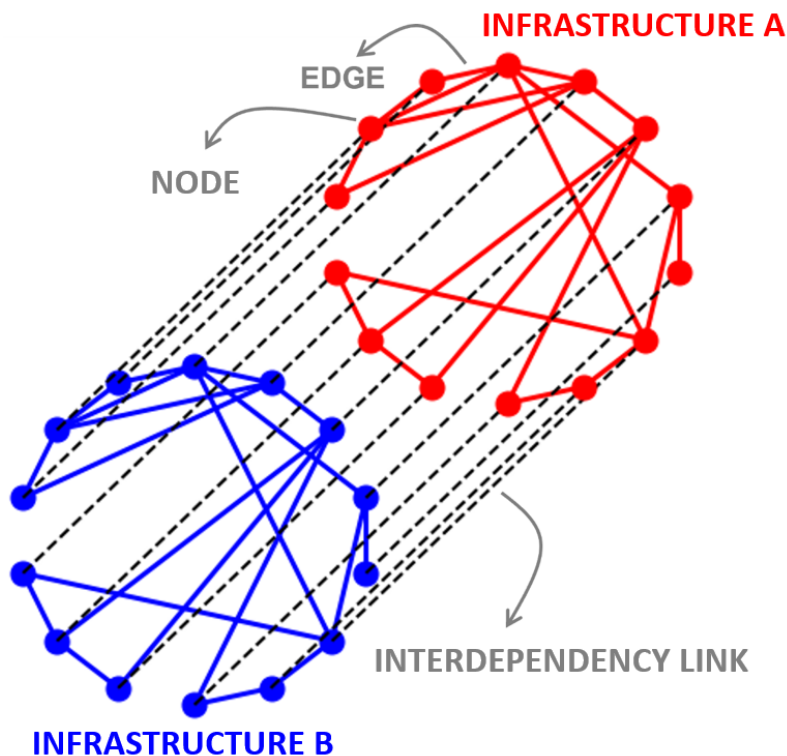


Figure 1: Network representation of two interdependent infrastructures. In evidence, we can notice the two structural components of networks (nodes and edges) and their connection (interdependency links). The ensemble of interdependency links is referred to as *coupling interface*.

In most of the existing literature on interdependent CIs, coupling interfaces are treated as a known parameter, and no optimization nor analysis is performed. Limited works try to optimize the design of the coupling interface (e.g. [7] or [8]); however, they rely on heuristic methods based on network science metrics, which do not guarantee optimal solutions nor high quality designs of coupling interface.

In this work, we propose a resilience-based mathematical framework, based on the *defender-attacker-defender* (DAD) model [10]–[13], for the optimal design of coupling interfaces in interdependent CIs. The DAD approach allows to identify solutions, in this case a coupling interface design, which are robust against the worst realization of uncertain scenarios, in this case failure scenarios.

In general, the motivations of this work are the following:

- *research*: the design of coupling interfaces between interdependent CIs has not been addressed comprehensively in the existing literature, and to the best of our knowledge, no mathemat-

ical programming approach has been proposed. As the coupling interface is a key factor of interdependent CIs and their resilience, optimizing its design is an important issue;

- *application*: due to the importance of coupling interface design, decision-makers and planners should be provided with the means and tools to evaluate and optimize the allocation of interdependency links between interdependent CIs.

As illustrative case-study, we rely on interdependent power and gas networks (IPGNs), similarly to [14], where gas networks need electricity for the functionality of their equipment (valves, pumps, compressors, etc.), and power networks need a gas supply to produce electricity in gas-fired power plants.

1.2. Related work

In the next sections we review the main works related to resilience enhancement in CIs, and design and optimization of coupling interfaces between interdependent CIs.

1.2.1. Resilience enhancement in critical infrastructures

The purpose of this section is to explain the main concepts in the context of resilience enhancement and give a general overview in order to better contextualize and position this work.

As critical infrastructures represent the backbone of essential societal functions, ensuring their resilience is a fundamental task [2]. The resilience of a system is defined as “*its ability to withstand stressors, adapt, and rapidly recover from disruptions*” [15]. Resilience refers to the behaviour of a system in disruptive conditions, it is generally represented with a resilience curve, as in Figure 2, and it is defined as the combination of three phases [2], [16]:

- the disturbance phase, which describes the speed and the severity of the disruption; this phase is strictly connected to the concepts of survivability and vulnerability¹;
- the degraded phase, which describes the temporal extension of the disruption after the disturbance phase, and it is linked to the emergency preparedness;
- the restoration phase, which describes the operations of restoration and repair.

The resilience of a system can be measured using different approaches, and various metrics are available in the existing literature [20]. A renowned approach is called $\Phi\Lambda E\Pi$ (pronounced “FLEP”) [16], and it consists of the computation of four different metrics:

¹Survivability is defined in [17] as “*the capability of a system to fulfill its mission in a timely manner in the presence of attacks, failures, or accidents*”, and it can be interpreted as the residual performance after the disturbance phase. Vulnerability is defined in [18] as “*degree of loss or damage to a system when exposed to a strain of a given type and magnitude*”, and it can be interpreted as the drop of performance due to the disturbance phase.

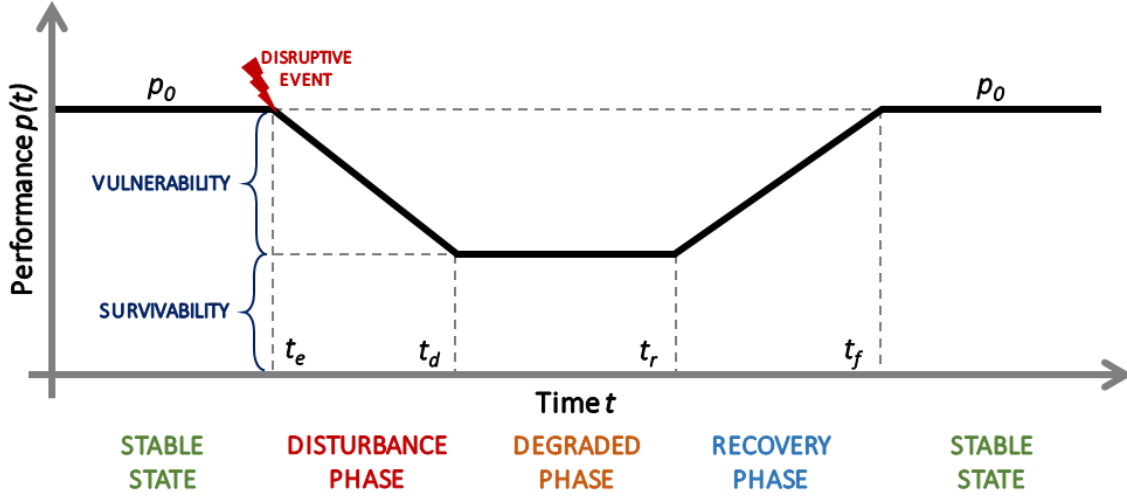


Figure 2: Qualitative representation of a resilience curve and the related phases [16], [19]

- Φ : it defines the rate of performance drop during the disturbance phase. Using Figure 2 as a reference, where $p(t)$ defines a performance indicator at time t , it can be computed as the difference in performance before and after the disruptive event divided by the duration of the event, as in Equation (1):

$$\Phi = \frac{p(t_e) - p(t_d)}{t_d - t_e}; \quad (1)$$

- Λ : it defines the magnitude of the drop in performance. This metric corresponds to the concept of vulnerability, and it is strictly correlated with the survivability. It can be computed as the difference in performance before and after the disruptive event, as in Equation (2)

$$\Lambda = p(t_e) - p(t_d); \quad (2)$$

- E : it defines the temporal extension of the degraded phase, and it can be computed as in (3):

$$E = t_r - t_d; \quad (3)$$

- Π : it defines the rate of recovery, and it can be computed as the difference in performance at the beginning and at the end of the recovery phase, divided by the duration of the recovery, as in Equation (4):

$$\Pi = \frac{p(t_f) - p(t_r)}{t_f - t_r}. \quad (4)$$

Enhancing the resilience of systems and infrastructures by optimizing design, preventive measures and resource allocation (e.g. transmission and/or generation expansion, protection of components, allocation of recovery resources, reliable network design, etc.), is one of the most important

tasks and a major topic in the field of critical infrastructures. Within this context, several works are available, and they can be distinguished according to different characteristics: *i*) which resilience phase is optimized; *ii*) which type of infrastructures is optimized; *iii*) which type of optimization model is used.

The optimization of critical infrastructures resilience can focus on one or multiple phases: for example, in [11] and [21], the resilience of power networks is enhanced by focusing separately on the optimization of protection against the disturbance phase and recovery phase, respectively; on the contrary, in [13] and [22], the resilience of interdependent CIs is enhanced by simultaneously optimizing both the disturbance phase and recovery phase.

An important feature that distinguishes the different works is which type of infrastructure is optimized, in terms of resilience. Several authors focus on resilience of single infrastructures, such as power networks [23] or water networks [24]. However, many other authors focus on the integrated optimization of resilience of multiple interdependent CIs, such as power and gas networks [25] or power and water networks [26], accounting for their mutual interdependencies when optimizing their resilience by preventive measures and resource allocation. The type of infrastructure under consideration is a key factor, as each infrastructure is characterized by specific operational models and interdependencies on other systems.

Another important difference within the existing works is the type of optimization model used for the resilience enhancement, which strongly impacts the quality and the nature of the solution. Many authors apply multi-level approaches, such as the DAD model [27], to enhance CIs resilience. These approaches offer robust solutions, and usually affordable computational cost. Some authors also include uncertainty using a stochastic optimization approach [28], in order to enhance the resilience expectation against a known probability distribution of uncertain parameters. Moreover, heuristics approach are also used [29], in order to derive high-quality solutions with operational models which can not be solved by traditional mathematical programming approaches.

It should be highlighted than in the aforementioned works the resilience of CIs is enhanced by optimizing different preventive measures and resource allocations, such as construction of new components (generation/expansion planning), protection of components or repair scheduling. However, the coupling interface, despite being a key parameter, is not optimized. As it is explained in the next section, only a limited number of works accounts for different coupling interface designs between interdependent CIs.

1.2.2. Design and optimization of coupling interface

When the state/functionality of one infrastructure depends on the state/functionality of another one, a relationship of interdependency exists. Interdependencies are unidirectional when one infras-

structure depends on another one, but not vice versa; otherwise, they are bidirectional [30], [31]. As interdependencies have been a subject of research since the early 2000s [2], different classifications exist in the literature [30]–[33]. One of the most used classifications is the one proposed in [30], where four categories are identified:

- *physical*, when one CI depends on another one through a physical flow (energy, goods, etc.);
- *cyber*, when one CI depends on another one through a flow of data and information;
- *geographic*, when elements of different infrastructures share the same location and they can be modified by a change in the environment conditions;
- *logical*, when a relationship which is not physical, cyber, or geographic exist.

CIs are often modeled with a network science approach [9], and the interdependencies are represented as links between components (nodes and/or edges) belonging to different infrastructures [34]. We refer to the ensemble of interdependency links as coupling interface. Its topology, i.e. where the interdependency links are present, plays a key role in terms of failure propagation between different infrastructures. Interdependency topology and design have been addressed in the field of interdependent networks, where various works focus on evaluating coupling interfaces and their impact on failure propagation [35], [36], and how coupling interfaces, if properly allocated, can increase the robustness of interdependent networks [37]–[39]. These works, despite representing a solid theoretical framework, mainly rely on percolation theory, and they fail to capture the details and the complex dynamics of real-world infrastructures.

Despite the critical role of coupling interfaces, in the existing literature they are often considered as a given parameter, and they are not analyzed nor optimized.

In some works, different network metric-based coupling strategies are tested on different interdependent CIs, such as power and water networks [40] or power and telecommunication networks [41]–[43]. In these works, the impact of different topologies is evaluated, and they demonstrate the importance of considering the coupling interface design problem within realistic CIs. However, these network-based heuristic approaches do not guarantee optimal solutions.

Similar network metrics-based approaches are also proposed in [7] and [8]. In [7], the authors propose an approach for designing coupling interfaces between urban CIs in order to increase their robustness against external attacks. The proposed strategy for designing the coupling interface is based on multiple network metrics (node degree, betweenness, clustering coefficient and Euclidean distance). In [8], the authors propose a similar approach, also accounting for physical features of the CIs, such as levels of supply and demand. However, these works still rely on network metrics as an heuristics. Consequently, they do not guarantee optimal solutions and the quality of the identified

coupling interface designs depends on the case-study considered. Moreover, these approaches are tailor-made and are not readily generalizable to other case-studies, as one specific heuristic strategy might perform well in some networks and poorly for other systems.

1.3. Contribution

In this work, a novel optimization-based approach for designing coupling interfaces between interdependent CIs is proposed. Our model ensures that coupling interface topologies are optimized in order to maximize the worst-case realization of combined performed of the interdependent infrastructures under random failures. The proposed approach is based on the DAD model, a three-stage sequential game which allows to identify robust defense strategies and/or resource allocation against a defined set of feasible attack scenarios. To demonstrate the validity of our approach, interdependent power and gas networks (IPGNs) are used as illustrative case-study.

The contributions of this papers can be summarized as follows:

- We developed a novel resilience-based optimization approach, which can be directly applied to design or retrofit new or existent coupling interfaces between interdependent CIs.
- We developed an approach for the optimization of coupling interface design that is generalizable for any case-study by selecting the appropriate operational model for the interdependent CIs.
- We demonstrated that our approach outperforms network metrics-based coupling interface strategies available in the existing literature.

The rest of this paper is organized as follows: in Section 2, the problem formulation is detailed; in Section 3, the solution strategy is explained; in Section 4, the illustrative case-study is detailed; in Section 5, results and discussion are presented; in Section 6, conclusive remarks and possible future developments are detailed.

2. Optimization problem formulation

2.1. Modeling framework

In this work, each infrastructure is modeled using a network flow-based approach [9], [44], where a network is a mathematical construct described by a graph $G = (V, E)$. The set V contains N nodes, connected by L edges, contained within the set E . Each edge k is directed and has an origin node $O(k)$ and a destination node $D(k)$. In line with a flow-based approach, we assume that commodities goods, and services are produced and consumed within nodes and distributed through

edges. Each node i has a production capacity \bar{p}_i and a requested demand \bar{d}_i , while each edge k has a flow capacity \bar{f}_k .

In this work, we focus on the combined performance P_C of the interdependent CIs [14], defined as in (5):

$$P_C = \sum_{h \in H} \frac{w_h}{\bar{d}_h} \sum_{i \in V_h} d_i \quad (5)$$

where the subscript H denotes the set of interdependent CIs, w_h represents the weight of infrastructure h when computing the combined performance, \bar{d}_h is the total requested demand of goods, services, or commodities in infrastructure h , and d_i is the supplied demand of goods, services, or commodities in each node i of infrastructure h .

Considering the resilience framework described in Section 1.2.1, the combined performance in conditions of disruption represents the concept of survivability of the interdependent CIs, complementary to the concept of vulnerability and to the Λ metric of the $\Phi\Lambda E\Pi$ approach. In this work, we do not consider the restoration phase, as it is characterized by deep uncertainties and it should be optimized case-by-case according to the specific disruption and failure scenarios [21].

As illustrative case-study, we consider interdependent power and gas networks (IPGNs), which are mutually interdependent on each other with physical interdependencies. In fact, equipment in the gas network, such as valves, compressors, or pumps, needs a constant power supply; power networks, if gas-fired power plants are present, need a constant supply of gas. The combined performance of the IPGNs can be defined as in Equation (6):

$$P_{C,IPGNs} = \frac{w_{PN}}{\bar{d}_{PN}} \sum_{i \in V_{PN}} d_i + \frac{w_{GN}}{\bar{d}_{GN}} \sum_{i \in V_{GN}} d_i \quad (6)$$

where the subscripts PN and GN denote the power network and gas network, respectively, w_{PN} and w_{GN} represent the weight of power network and gas network when computing the combined performance², \bar{d}_{PN} and \bar{d}_{GN} are the total requested demand of power and gas, and d_i is the supplied power or gas in each node of the networks. The combined performance P_C ranges from 0, when no power and gas demand is supplied, to 1, when 100% of the requested demand of power and gas is supplied.

In the power network, nodes represent buses, while edges represent power lines; in the gas network, nodes represent hubs, while edges represent gas pipelines. The power network operations are simulated with a DC power flow model, while the gas network operations are simulated with a linear maximal flow model, which is a suitable approximation of flow-based infrastructures [14], [45]–[47].

²It should be noted that $w_{PN} + w_{GN} = 1$.

Several works analyze critical infrastructures in the context of specific types of hazards, like intentional attacks [46], spatially-localized attacks [48] and extreme natural events [14], [49]. In this work, we adopt an approach based on the maximum number of contingencies [27], [50]. For simplicity, but without loss of generality, we assume that only transmission lines (edges) in the power network can be attacked and failed. By considering the simultaneous failures of transmission lines, the present model is agnostic about the source of disruption, providing a rapid and objective way of calculating the consequence of damage to any set of components.

In this work, the following assumptions are considered:

- a single demand scenario is considered, i.e. the expected forecast of requested power and gas demand [27];
- each node in the gas network needs to receive a power supply from the power network in order to run equipment;
- each node in the power network with some production capacity is assumed to contain a gas-fired power plant and needs to receive a gas supply from the gas network;
- each node in the power network can be dependent on one, and only one node in the gas network, and vice versa;
- allocating the coupling interface has a cost that depends on the geographical distance between the two nodes connected by the interdependency link;
- the operators are perfectly aware of the status of the components within the power network and gas network [27].

The purpose of the proposed model is to design a coupling interface between IPGNs that ensures satisfactory combined performance in normal conditions (no failures) and conditions of disruption.

2.2. Defender-attacker-defender approach

The problem takes the form of a trilevel DAD optimization model, a formulation often used in the framework of optimization of defense strategies and resources in CIs (e.g. [10], [14], [27]). It is useful to imagine the problem as a three-players game: the inner defender aims at maximizing the combined performance of the IPGNs through the operational variables of the two systems; the middle attacker aims at minimizing the combined performance choosing the most disruptive attack plan; the outer defender aims at maximizing the combined performance of the IPGNs by designing a robust coupling interface that also ensures satisfactory performance in normal conditions (no failures). The full formulation is shown in (7)-(43):

$$\begin{aligned}
& \max_{\substack{\mathbf{p}', \mathbf{d}', \mathbf{f}', \boldsymbol{\theta}', \boldsymbol{\delta}' \\ \mathbf{y}^{g \leftarrow p} \in \{0,1\}^{N_C} \\ \mathbf{y}^{p \leftarrow g} \in \{0,1\}^{N_C}}} \min_{\mathbf{u} \in \{0,1\}^{L_{PN}}} \max_{\mathbf{p}, \mathbf{d}, \mathbf{f}, \boldsymbol{\theta}, \boldsymbol{\delta}} \frac{w_{PN}}{\bar{d}_{PN}} \sum_{i \in V_{PN}} d_i + \frac{w_{GN}}{\bar{d}_{GN}} \sum_{i \in V_{GN}} d_i \\
& - \gamma \left(\sum_{\substack{i \in V_{GN} \\ j \in V_{PN}}} y_{ij}^{g \leftarrow p} d_{ij}^{km} c_{km}^{g \leftarrow p} + \sum_{\substack{i \in V_{PN} \\ j \in V_{GN}}} y_{ij}^{p \leftarrow g} d_{ji}^{km} c_{km}^{p \leftarrow g} \right) \tag{7}
\end{aligned}$$

subject to:

First level

$$\sum_{j \in V_{PN}} y_{ij}^{g \leftarrow p} \leq 1, \quad \forall i \in V_{GN} \tag{8}$$

$$\sum_{j \in V_{GN}} y_{ij}^{p \leftarrow g} \leq 1, \quad \forall i \in V_{PN} \tag{9}$$

$$\sum_{\substack{i \in V_{GN} \\ j \in V_{PN}}} y_{ij}^{g \leftarrow p} d_{ij}^{km} c_{km}^{g \leftarrow p} + \sum_{\substack{i \in V_{PN} \\ j \in V_{GN}}} y_{ij}^{p \leftarrow g} d_{ji}^{km} c_{km}^{p \leftarrow g} \leq B_{ci} \tag{10}$$

$$\frac{w_{PN}}{\bar{d}_{PN}} \sum_{i \in V_{PN}} d_i + \frac{w_{GN}}{\bar{d}_{GN}} \sum_{i \in V_{GN}} d_i \geq 1 \tag{11}$$

$$0 \leq p'_i \leq \bar{p}_i, \quad \forall i \in V_{TOT} \tag{12}$$

$$0 \leq d'_i \leq \bar{d}_i + \sum_{j \in V_{GN}} y_{ji}^{g \leftarrow p} \bar{d}_j^{MW}, \quad \forall i \in V_{PN} \tag{13}$$

$$0 \leq d'_i \leq \bar{d}_i + \sum_{j \in V_{PN}} y_{ji}^{p \leftarrow g} \bar{d}_j^{n^3}, \quad \forall i \in V_{GN} \tag{14}$$

$$-\bar{f}_k \leq f'_k \leq \bar{f}_k, \quad \forall k \in E_{TOT} \tag{15}$$

$$x_k f'_k - (\theta'_{O(k)} - \theta'_{D(k)}) = 0, \quad \forall k \in E_{PN} \tag{16}$$

$$p'_i - d'_i + \sum_{k|D(k)=i} f'_k - \sum_{k|O(k)=i} f'_k = 0, \quad \forall i \in V_{TOT} \tag{17}$$

$$d_i - \delta_i^{p'} \left(\bar{d}_i^b + \sum_{j \in V_{GN}} y_{ji}^{g \leftarrow p} \bar{d}_j^{MW} \right) \geq 0, \quad \forall i \in V_{PN} \quad (18)$$

$$d'_i - \delta_i^{g'} \left(\bar{d}_i^b + \sum_{j \in V_{PN}} y_{ji}^{p \leftarrow g} \bar{d}_j^{m^3} \right) \geq 0, \quad \forall i \in V_{GN} \quad (19)$$

$$p'_i - \bar{p}_i \sum_{j \in V_{GN}} y_{ij}^{p \leftarrow g} \delta_j^{g'} \leq 0, \quad \forall i \in V_{PN} \quad (20)$$

$$p'_i - \bar{p}_i \sum_{j \in V_{PN}} y_{ij}^{g \leftarrow p} \delta_j^{p'} \leq 0, \quad \forall i \in V_{GN} \quad (21)$$

$$d'_i - \left(\bar{d}_i^b + \sum_{j \in V_{PN}} y_{ji}^{p \leftarrow g} \bar{d}_j^{m^3} \right) \sum_{j \in V_{PN}} y_{ij}^{g \leftarrow p} \delta_j^{p'} \leq 0, \quad \forall i \in V_{GN} \quad (22)$$

$$- \sum_{\substack{k|O(k=i) \\ j \in V_{PN}}} y_{ij}^{g \leftarrow p} \delta_i^{p'} \bar{f}_k \leq f'_k \leq \sum_{\substack{k|O(k=i) \\ j \in V_{PN}}} y_{ij}^{g \leftarrow p} \delta_i^{p'} \bar{f}_k, \quad \forall k \in E_{GN} \quad (23)$$

$$- \sum_{\substack{k|D(k=i) \\ j \in V_{PN}}} y_{ij}^{g \leftarrow p} \delta_i^{p'} \bar{f}_k \leq f'_k \leq \sum_{\substack{k|D(k=i) \\ j \in V_{PN}}} y_{ij}^{g \leftarrow p} \delta_i^{p'} \bar{f}_k, \quad \forall k \in E_{GN} \quad (24)$$

$$y_{ji}^{g \leftarrow p} \in \{0, 1\}, \quad y_{ji}^{p \leftarrow g} \in \{0, 1\}, \quad \forall i \in V_{PN}, \forall j \in V_{GN} \quad (25)$$

$$\delta_i^{p'} \in \{0, 1\}, \quad \delta_j^{g'} \in \{0, 1\}, \quad \forall i \in V_{PN}, \forall j \in V_{GN} \quad (26)$$

Second level

$$\sum_{k \in E_{PN}} (1 - u_k) \leq K_{att} \quad (27)$$

$$u_k \in \{0, 1\}, \quad \forall k \in E_{PN} \quad (28)$$

Third level

$$0 \leq p_i \leq \bar{p}_i, \quad \forall i \in V_{TOT} \quad (29)$$

$$0 \leq d_i \leq \bar{d}_i^b + \sum_{j \in V_{GN}} y_{ji}^{g \leftarrow p} \bar{d}_j^{MW}, \quad \forall i \in V_{PN} \quad (30)$$

$$0 \leq d_i \leq \bar{d}_i^b + \sum_{j \in V_{PN}} y_{ji}^{p \leftarrow g} \bar{d}_j^{m^3}, \quad \forall i \in V_{GN} \quad (31)$$

$$-u_k \bar{f}_k \leq f_k \leq u_k \bar{f}_k, \quad \forall k \in E_{PN} \quad (32)$$

$$-\bar{f}_k \leq f_k \leq \bar{f}_k, \quad \forall k \in E_{GN} \quad (33)$$

$$(x_k f_k - (\theta_{O(k)} - \theta_{D(k)})) u_k = 0, \quad \forall k \in E_{PN} \quad (34)$$

$$p_i - d_i + \sum_{k|D(k)=i} f_k - \sum_{k|O(k)=i} f_k = 0, \quad \forall i \in V_{TOT} \quad (35)$$

$$d_i - \delta_i^p \left(\bar{d}_i^b + \sum_{j \in V_{GN}} y_{ji}^{g \leftarrow p} \bar{d}_j^{MW} \right) \geq 0, \quad \forall i \in V_{PN} \quad (36)$$

$$d_i - \delta_i^g \left(\bar{d}_i^b + \sum_{j \in V_{PN}} y_{ji}^{p \leftarrow g} \bar{d}_j^{m^3} \right) \geq 0, \quad \forall i \in V_{GN} \quad (37)$$

$$p_i - \bar{p}_i \sum_{j \in V_{GN}} y_{ij}^{p \leftarrow g} \delta_j^g \leq 0, \quad \forall i \in V_{PN} \quad (38)$$

$$p_i - \bar{p}_i \sum_{j \in V_{PN}} y_{ij}^{g \leftarrow p} \delta_j^p \leq 0, \quad \forall i \in V_{GN} \quad (39)$$

$$d_i - \left(\bar{d}_i^b + \sum_{j \in V_{PN}} y_{ji}^{p \leftarrow g} \bar{d}_j^{m^3} \right) \sum_{j \in V_{PN}} y_{ij}^{g \leftarrow p} \delta_j^p \leq 0, \quad \forall i \in V_{GN} \quad (40)$$

$$- \sum_{\substack{k|O(k)=i \\ j \in V_{PN}}} y_{ij}^{g \leftarrow p} \delta_i^p \bar{f}_k \leq f_k \leq \sum_{\substack{k|O(k)=i \\ j \in V_{PN}}} y_{ij}^{g \leftarrow p} \delta_i^p \bar{f}_k, \quad \forall k \in E_{GN} \quad (41)$$

$$- \sum_{\substack{k|D(k)=i \\ j \in V_{PN}}} y_{ij}^{g \leftarrow p} \delta_i^p \bar{f}_k \leq f_k \leq \sum_{\substack{k|D(k)=i \\ j \in V_{PN}}} y_{ij}^{g \leftarrow p} \delta_i^p \bar{f}_k, \quad \forall k \in E_{GN} \quad (42)$$

$$\delta_i^p \in \{0, 1\}, \quad \delta_j^g \in \{0, 1\}, \quad \forall i \in V_{PN}, \forall j \in V_{GN}. \quad (43)$$

Equation (7) is the objective function of the trilevel optimization problem, and it contains three terms. The first two terms correspond to the combined performance P_C , previously shown in

Equation (6). By including P_C in the objective function, we can identify a coupling interface that maximizes the combined performance of the IPGNs in the worst failure scenario; in other words, we can identify the coupling interface that maximizes the survivability of the IPGNs (or minimizes the Λ resilience metric) of the IPGNs in the worst failure scenario. The power and gas supplied to each node i are defined by the variables d_i , while the total requested demand of power and gas, denoted as \bar{d}_{PN} and \bar{d}_{GN} , are constant parameters computed as in (44) and (45), respectively.

$$\bar{d}_{PN} = \sum_{i \in V_{PN}} \bar{d}_i^b + \sum_{j \in V_{GN}} \bar{d}_j^{MW} \quad (44)$$

$$\bar{d}_{GN} = \sum_{i \in V_{GN}} \bar{d}_i^b + \sum_{j \in V_{PN}} \bar{d}_j^{m^3} \quad (45)$$

In these equations, the constant \bar{d}_i^b denotes the baseline requested demand of power or gas in each node, and it represents the consumption of various private and public consumers. The constant \bar{d}_j^{MW} denotes the requested power demand of node $j \in V_{GN}$, while the constant $\bar{d}_j^{m^3}$ denotes the requested gas demand of node $j \in V_{PN}$.

The third term of the objective function ensures that, if more than one optimal coupling interface exists, the one with the lowest allocation cost is chosen. The terms within the parentheses define the cost of allocating a specific coupling interface. The binary variable $y_{ij}^{g \leftarrow p} = 1$ if an interdependency link from node $j \in V_{PN}$ to node $i \in V_{GN}$ is allocated, and $y_{ij}^{g \leftarrow p} = 0$ otherwise. Similarly, the binary variable $y_{ij}^{p \leftarrow g} = 1$ if an interdependency link from node $j \in V_{GN}$ to node $i \in V_{PN}$ is allocated, and $y_{ij}^{p \leftarrow g} = 0$ otherwise. The constant d_{ij}^{km} denotes the distance in kilometer between node $i \in V_{GN}$ and node $j \in V_{PN}$, while the constants $c_{km}^{g \leftarrow p}$ and $c_{km}^{p \leftarrow g}$ denote the cost per kilometer of allocating an interdependency link from the power network to the gas network, and from the gas network to the power network, respectively. The terms within the parentheses are multiplied by a factor γ , which represents a very small number. This factor ensures that the priority within the optimization is given to the combined performance P_C .

Equations (8)-(26) denote the constraints of the first optimization level, corresponding to the outer defender. This agent allocates the coupling interface in a way such that: *i*) the available monetary budget B_{ci} is respected, as shown in Constraint (10), and *ii*) in normal conditions (no failures), it is possible to supply the whole requested demand of power and gas ($P_C=1$). Consistently with the existing literature, we assume that each node in the gas network can be dependent on, and connected through an interdependency link to, only one node in the power network, and vice versa. We refer to this as the *single-dependency* assumption, and it is enforced by Constraints (8) and (9). The coupling interface, as previously explained, is allocated through the binary variables $y_{ij}^{g \leftarrow p}$ and $y_{ij}^{p \leftarrow g}$, contained within the vectors $\mathbf{y}^{g \leftarrow p}$ and $\mathbf{y}^{p \leftarrow g}$ with dimension $N_C = N_{PN} \times N_{GN}$.

The coupling interface must be allocated in order to guarantee that, in normal conditions, the requested demand of power and gas is fully satisfied, as enforced by Constraint (11). This condition depends on the first-level operational variables, contained within the vectors \mathbf{p}' , \mathbf{d}' , \mathbf{f}' , $\boldsymbol{\theta}'$, $\boldsymbol{\delta}'$, which represent production levels, supply demands, flows, phase angles, and interdependency links status, respectively³.

Equations (12)-(26) contain the operational constraints of the first level. For both networks, the production level of power or gas p'_i in each node i is limited by the production capacity \bar{p}_i , as enforced in Constraint (12). Similarly, as shown in Constraints (13) and (14), the supplied demand of power or gas d'_i in each node i is limited by the requested demand. As it is shown on the right side of (13), the requested power demand of node $i \in V_{PN}$ is given by the sum of the baseline requested power demand \bar{d}_i^b and all the requested power demands \bar{d}_j^{MW} of the nodes $j \in V_{GN}$ which depend on the node $i \in V_{PN}$ for the electricity supply ($y_{ji}^{g \leftarrow p} = 1$). Similarly, as it is shown on the right side of (14), the requested gas demand of node $i \in V_{GN}$ is given by the sum of the baseline requested gas demand \bar{d}_i^b and all the requested gas demands \bar{d}_j^{m3} of the nodes $j \in V_{PN}$ which depend on the node $i \in V_{GN}$ for the gas supply ($y_{ji}^{p \leftarrow g} = 1$).

The flow of power and gas f'_k in each edge k is limited, in absolute value, by the flow capacity \bar{f}_k , as shown in Constraint (15). Moreover, in each line of the power network, the power flow is subject to the DC power flow assumption, enforced by Constraint (16), where x_k represents the reactance of line k , and $\theta'_{O(k)}$ and $\theta'_{D(k)}$ are the phase angles in the origin and destination node of line k , respectively.

The net nodal balance of power and gas in each node is ensured by Constraint (17).

The operations of the IPGNs depends on the status of the interdependency links. Similarly to other existing works (e.g. [14]), we assume a binary functional status for the interdependency links (1 if functional, 0 if not functional). We assume that the binary functional status of each interdependency link starting from node $i \in V_{PN}$ is expressed by the binary variable $\delta_i^{p'}$; similarly, the binary functional status of each interdependency link starting from node $i \in V_{GN}$ is expressed by the binary variable $\delta_i^{g'}$. Each interdependency link starting from node $i \in V_{PN}$ is functional ($\delta_i^{p'} = 1$) only if the requested power demand in i is fully satisfied, as enforced in Constraint (18). The rationale behind this assumption is that, if some electricity is not supplied to i , the dependent nodes within the gas network might not receive the necessary electricity. As shown in Constraint (19), the same assumption is taken for the interdependency link starting from the gas network, with a similar rationale: each interdependency link starting from node $i \in V_{GN}$ is functional ($\delta_i^{g'} = 1$) only if the requested gas demand in i is fully satisfied. These assumption are consistent with the

³The superscript ' denotes the operational variables of the first level.

existing literature (e.g. [14]). However, different assumptions which are not included in this work, such as multi-discrete or continuous status for the interdependency links, can be implemented by appropriate changes of the variables δ' .

We assume that the electricity in the power network is produced by gas-fired power plants, and in each node $i \in V_{PN}$ it is possible to produce power only if a functional interdependency link with a node $j \in V_{GN}$ is present ($y_{ij}^{p \leftarrow g} = 1$ and $\delta_j^{g'} = 1$). This condition is enforced by Constraint (20).

We assume that gas in the gas network can be extracted (produced) and supplied only if there is enough electricity. Therefore, in each node $i \in V_{GN}$ it is possible to produce and supply gas only if a functional interdependency link with a node $j \in V_{PN}$ is present ($y_{ij}^{g \leftarrow p} = 1$ and $\delta_j^{p'} = 1$). These conditions are enforced by Constraints (21) and (22). Moreover, we assume that gas can flow in a pipe k only if both the origin and destination nodes present a functional interdependency link with a node $j \in V_{PN}$, as enforced by Constraints (23) and (24).

Equations (27) and (28) denote the constraints of the second level of the optimization problem, corresponding to the attacker. This agent decides which lines of the power network to target and fail through the binary variables u_k , contained within the vector \mathbf{u} . Each variable u_k takes the value 0 if line k is targeted and failed, and value 1 otherwise. The attacker can target and fail a maximum number K_{att} of lines in the power network, as shown in Constraint (27).

Equations (29)-(43) contain the operational constraints of the third level, corresponding to the inner defender. This agent aims at maximizing the combined performance of the IPGNs through the operational variables of the third level, contained within the vectors $\mathbf{p}, \mathbf{d}, \mathbf{f}, \boldsymbol{\theta}, \boldsymbol{\delta}$.

Constraints (29)-(43) are equivalent to the previously-explained Constraints (8)-(26). However, in the third level, we also account for the failures of power lines through the inclusion of binary variables u_k in Constraints (32) and (34). Constraint (32) ensures that the power flow in a failed power line is 0. Constraints (34) ensures that the DC power flow assumption is maintained in functional power lines and disregarded in failed power lines. Constraint (34) contains quadratic terms due to the multiplication of the binary variable u_k with the continuous variables f_k and θ_i . These quadratic terms can be linearized with a ‘‘Big-M’’ approach, as shown in Appendix A. The other constraints in (29)-(43) are equivalent to the ones in (8)-(26).

For simplicity, we can express the optimization problem in (7)-(43) with the compact matrix formulation in (46)-(51).

$$\max_{\substack{\mathbf{h}', \boldsymbol{\delta}' \\ \mathbf{y}^{g \leftarrow p} \in \{0,1\}^{N_C} \\ \mathbf{y}^{p \leftarrow g} \in \{0,1\}^{N_C}}} \min_{\mathbf{u} \in \{0,1\}^{L_{PN}}} \max_{\mathbf{h}, \boldsymbol{\delta}} \mathbf{b}^T \mathbf{h} + \mathbf{c}^T \mathbf{y} \quad (46)$$

subject to:

$$\mathbf{P}\mathbf{y} \leq \mathbf{g} \quad (47)$$

$$\mathbf{b}^T \mathbf{h}' \geq 1 \quad (48)$$

$$\mathbf{R}'\mathbf{h}' \leq \mathbf{q}' - \mathbf{H}'\mathbf{y} - \mathbf{W}'\boldsymbol{\delta}' - \mathbf{y}^T \mathbf{D}'\boldsymbol{\delta}' \quad (49)$$

$$\mathbf{K}\mathbf{u} \leq \mathbf{a} \quad (50)$$

$$\mathbf{R}\mathbf{h} \leq \mathbf{q} - \mathbf{T}\mathbf{u} - \mathbf{H}\mathbf{y} - \mathbf{W}\boldsymbol{\delta} - \mathbf{y}^T \mathbf{D}\boldsymbol{\delta}. \quad (51)$$

The vectors \mathbf{h}' and \mathbf{h} contain the continuous variables of the first and third level, respectively. The other variable vectors, \mathbf{y} , $\boldsymbol{\delta}'$, and $\boldsymbol{\delta}$, contain binary variables (vector \mathbf{y} contains vectors $\mathbf{y}^{g \leftarrow p}$ and $\mathbf{y}^{p \leftarrow g}$). The vectors \mathbf{b} and \mathbf{c} contains the objective function coefficients, while the vectors \mathbf{g} , \mathbf{a} and \mathbf{q} contain constraint parameters. The matrices \mathbf{P} , \mathbf{R}' , \mathbf{H}' , \mathbf{W}' , \mathbf{D}' , \mathbf{K} , \mathbf{R} , \mathbf{H} , \mathbf{W} , and \mathbf{D} contain constraint coefficients with suitable dimensions.

Equation (46) corresponds to Equation (7); Equation (47) corresponds to Equations (8)-(10); Equation (48) corresponds to Equation (11); Equation (49) corresponds to Equations (12)-(26); Equation (50) corresponds to Equations (27)-(28); Equation (51) corresponds to Equations (29)-(43).

The optimal objective value of the trilevel optimization is the maximized combined performance of the IPGNs in the worst scenario within the set of feasible failure scenarios. An important output of the optimization problem is the optimal coupling interface design $\hat{\mathbf{y}}$.

3. Solution strategy

3.1. Linearization

As the problem in (46)-(51) (or equivalently (7)-(43)) contains several nonlinear terms, the first step of our solution strategy involves a reformulation into an equivalent linear form. In particular, the nonlinear terms arise from the multiplications of binary variables \mathbf{y}' and $\boldsymbol{\delta}'$ in (49), and \mathbf{y} and $\boldsymbol{\delta}$ in (51). Products of binary variables can be easily linearized by introducing new binary variables and additional constraints. Generally, the product of two binary variables a and b is also a binary variable, here called c , subject to Constraints (52)-(54):

$$c \leq a \quad (52)$$

$$c \leq b \quad (53)$$

$$c \geq a + b - 1. \quad (54)$$

The multiplications of \mathbf{y}' and $\boldsymbol{\delta}'$ in (49), and \mathbf{y} and $\boldsymbol{\delta}$ in (51), can then be linearized by introducing binary variables \mathbf{z} and \mathbf{r} and additional constraints of the type in (52)-(54). The variables \mathbf{z} are introduced to linearize the multiplication between two binary variables, while the variables \mathbf{r} are introduced to linearize the multiplication between three binary variables. Constraint (49) can then be replaced by Constraints (55) and (56), while Constraint (51) can then be replaced by Constraints (57) and (58):

$$\mathbf{R}'\mathbf{h}' \leq \mathbf{q}' - \mathbf{H}'\mathbf{y} - \mathbf{W}'\boldsymbol{\delta}' - \mathbf{S}'\mathbf{z}' - \mathbf{V}'\mathbf{r}' \quad (55)$$

$$\mathbf{Q}'\mathbf{z}' + \mathbf{F}'\mathbf{r}' \leq \mathbf{t}' - \mathbf{L}'\mathbf{y} - \mathbf{J}'\boldsymbol{\delta}' \quad (56)$$

$$\mathbf{R}\mathbf{h} \leq \mathbf{q} - \mathbf{T}\mathbf{u} - \mathbf{H}\mathbf{y} - \mathbf{W}\boldsymbol{\delta} - \mathbf{S}\mathbf{z} - \mathbf{V}\mathbf{r} \quad (57)$$

$$\mathbf{Q}\mathbf{z} + \mathbf{F}\mathbf{r} \leq \mathbf{t} - \mathbf{L}\mathbf{y} - \mathbf{J}\boldsymbol{\delta} \quad (58)$$

where Equations (56) and (58) corresponds to the additional constraints of the type in (52)-(54).

The linear compact matrix formulation corresponds to Equation (46) subject to (47)-(48), (50), and (55)-(58).

3.2. Nested Column&Constraint Generation algorithm

The presence of the binary variables $\boldsymbol{\delta}$ in the third stage makes it impossible to merge the second and third stage into a single minimization problem relying on the dual formulation. Therefore, we adopt a cutting plane strategy, called Nested Column&Constraint Generation (NC&CG) algorithm. It represents an exact method, with proven convergence to the global optimum, for solving multi-level mixed-integer linear programming with recourse problems [51], [52].

Figure 3 details the flowchart with the main steps of the NC&CG algorithm. In order to adopt this strategy, the original trilevel max-min-max problem is transformed into a max-min-max-max problem, by separating binary and continuous variables in the original third stage [14]. The new fourth stage contains only continuous variables, and it is then a pure LP problem. The formulation is then transformed into a max-min-max-min through a dual reformulation of the last stage. In this form, the problem can be solved using a NC&CG algorithm, identifying an outer and inner layer which exchange primal variables in form of parameters until the convergence to the global optimum is reached.

For a more detailed explanation of the C&CG algorithm, the reader is referred to [51], [52] for a theoretical framework and [14], [27], [50] for applications.

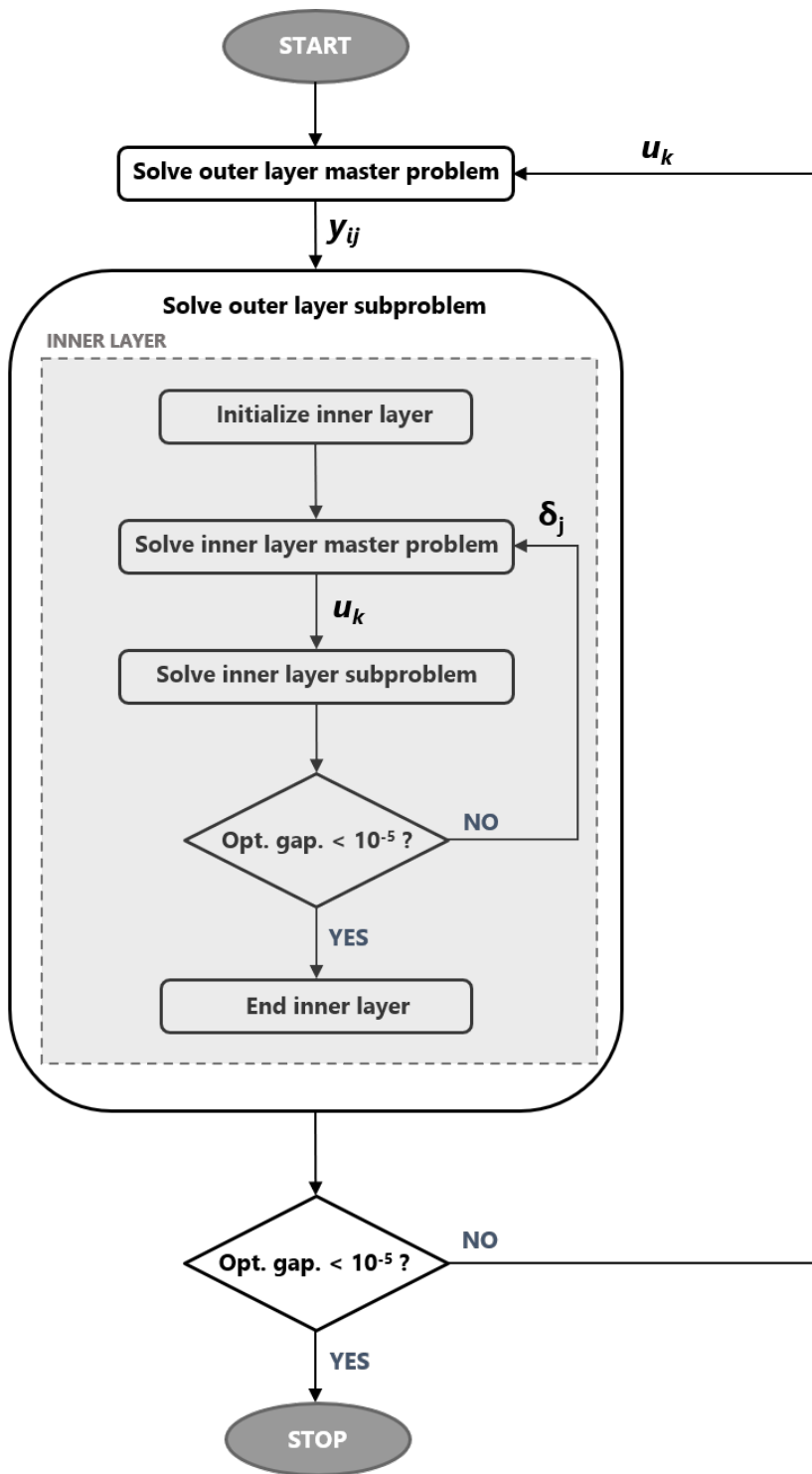


Figure 3: Flowchart of the NC&CG algorithm [14], [27].

3.3. Inner layer

The inner layer consists in solving the second and third level (min-max) in (46) with a fixed coupling interface \mathbf{y}^* . The output of the model is the worst-case realization of the combined performance and the associated optimal attack plan $\hat{\mathbf{u}}$. With fixed binary variables (coupling interface \mathbf{y}^* , interdependency variables $\boldsymbol{\delta}^*$ and attack plan \mathbf{u}^*), the inner-most maximization in (46) and the relative constraints take the form in (59)-(60):

$$\max_{\mathbf{h}} \mathbf{b}^T \mathbf{h} + \mathbf{c}^T \mathbf{y}^* \quad (59)$$

subject to :

$$\mathbf{R}\mathbf{h} \leq \mathbf{q} - \mathbf{T}\mathbf{u}^* - \mathbf{H}\mathbf{y}^* - \mathbf{W}\boldsymbol{\delta}^* - \mathbf{y}^{*T}\mathbf{D}\boldsymbol{\delta}^* \quad (60)$$

The problem in (59)-(60) is a pure LP, and thus the introduction of variables \mathbf{z} and \mathbf{r} is not necessary. Thanks to its linear nature, strong duality holds and it can be transformed into its dual form in (61)-(62):

$$\min_{\boldsymbol{\lambda}} (\mathbf{q} - \mathbf{T}\mathbf{u}^* - \mathbf{H}\mathbf{y}^* - \mathbf{W}\boldsymbol{\delta}^* - \mathbf{y}^{*T}\mathbf{D}\boldsymbol{\delta}^*)^T \boldsymbol{\lambda} \quad (61)$$

subject to:

$$\mathbf{R}^T \boldsymbol{\lambda} = \mathbf{b} \quad (62)$$

As the variables $\boldsymbol{\delta}$ are binary, the number of possible combinations that they can take is equal to 2^{N_δ} , where $N_\delta = N_{PN} + N_{GN}$ is the number of binary variables $\boldsymbol{\delta}$. We denote as \mathcal{D} the set containing all the possible combinations of binary variables $\boldsymbol{\delta}$. The C&CG approach exploits the observation that only a partial subset $\mathcal{D}_{part} \subseteq \mathcal{D}$ is essential to compute the optimal solution. The bilevel min-max formulation can be solved by iteratively reconstructing the partial set \mathcal{D}_{part} by following these steps:

1. Set $j = 0$, lower bound $LB_{in} = 0$, upper bound $UB_{in} = \infty$, and $\mathcal{D}_{part} = \emptyset$
2. Solve the inner master problem in Equations (63)-(66). Obtain an optimal solution $\hat{\rho}^{(j)}$ and optimal attack plan $\hat{\mathbf{u}}^{(j)}$. Update $LB_{in} = \hat{\rho}^{(j)} + \mathbf{c}^T \mathbf{y}^*$.

$$\min_{\rho, \mathbf{u}, \boldsymbol{\lambda}} \rho \quad (63)$$

subject to:

$$\rho \geq (\mathbf{q} - \mathbf{T}\mathbf{u} - \mathbf{H}\mathbf{y}^* - \mathbf{W}\boldsymbol{\delta}^{*(j)} - \mathbf{y}^{*T}\mathbf{D}\boldsymbol{\delta}^{*(j)})^T \boldsymbol{\lambda}^{(j)}, \quad \forall \boldsymbol{\delta}^{*(j)} \in \mathcal{D}_{part} \quad (64)$$

$$\mathbf{R}^T \boldsymbol{\lambda}^{(j)} = \mathbf{b}, \quad \forall \boldsymbol{\delta}^{*(j)} \in \mathcal{D}_{part} \quad (65)$$

$$\sum_{k \in E_{PN}} (1 - u_k) \leq K_{att} \quad (66)$$

3. Solve the inner subproblem in Equations (67)-(68) with $\hat{\mathbf{u}}^{(j)} = \mathbf{u}^*$. Obtain an optimal solution $\mathbf{b}^T \hat{\mathbf{h}}^{(j)}$ and $\hat{\boldsymbol{\delta}}^{(j)}$. Set $UB_{in} = \min(UB_{in}, \mathbf{b}^T \hat{\mathbf{h}}^{(j)} + \mathbf{c}^T \mathbf{y}^*)$.

$$\max_{\mathbf{h}, \boldsymbol{\delta}} \mathbf{b}^T \mathbf{h} \quad (67)$$

subject to :

$$\mathbf{R}\mathbf{h} \leq \mathbf{q} - \mathbf{T}\mathbf{u}^* - \mathbf{H}\mathbf{y}^* - \mathbf{W}\boldsymbol{\delta} - \mathbf{y}^{*T} \mathbf{D}\boldsymbol{\delta} \quad (68)$$

4. If $(UB_{in} - LB_{in})/UB_{in} < 10^{-5}$, $\hat{\mathbf{u}}^{(j)}$ represents the optimal attack and the algorithm can be terminated. Otherwise, $\mathcal{D}_{part} = \mathcal{D}_{part} \cup \hat{\boldsymbol{\delta}}^{(j)}$. Set $j \leftarrow j + 1$ and return to step 2.

The optimal attack plan, or, in other words, the feasible combination of variables \mathbf{u} which minimizes the combined performance for a fixed coupling interface \mathbf{y}^* , and the optimal value of the objective function represent the main outputs of the algorithm.

3.4. Outer layer

Similarly, the outer layer is solved by employing a partial set of attack scenarios $\mathcal{A}_{part} \subseteq \mathcal{A}$. The outer layer solves a bilevel max-min problem, and the minimization is solved by the inner layer algorithm.

The outer layer is solved by employing the following steps:

1. Set $j = 0$, lower bound $LB_{out} = 0$, upper bound $UB_{out} = \infty$, and $\mathcal{A}_{part} = \emptyset$
2. Solve the outer master problem in Equations (69)-(76). Obtain an optimal solution $\hat{\eta}^{(j)} + \mathbf{c}^T \hat{\mathbf{y}}^{(j)}$ and optimal coupling interface $\hat{\mathbf{y}}^{(j)}$. Update $UB_{out} = \min(UB_{out}, \hat{\eta}^{(j)} + \mathbf{c}^T \hat{\mathbf{y}}^{(j)})$

$$\max_{\substack{\eta, \mathbf{h}^{(j)} \\ \mathbf{h}', \boldsymbol{\delta}' \\ \mathbf{y} \in \{0,1\}}} \eta + \mathbf{c}^T \mathbf{y} \quad (69)$$

$$\eta \leq \mathbf{b}^T \mathbf{h}^{(j)}, \quad \forall \mathbf{u}^{*(j)} \in \mathcal{A}_{part} \quad (70)$$

$$\mathbf{P}\mathbf{y} \leq \mathbf{g} \quad (71)$$

$$\mathbf{b}^T \mathbf{h}' \geq 1 \quad (72)$$

$$\mathbf{R}'\mathbf{h}' \leq \mathbf{q}' - \mathbf{H}'\mathbf{y} - \mathbf{W}'\boldsymbol{\delta}' - \mathbf{S}'\mathbf{z}' - \mathbf{V}'\mathbf{r}' \quad (73)$$

$$\mathbf{Q}'\mathbf{z}' + \mathbf{F}'\mathbf{r}' \leq \mathbf{t}' - \mathbf{L}'\mathbf{y} - \mathbf{J}'\boldsymbol{\delta}' \quad (74)$$

$$\mathbf{R}\mathbf{h}^{(j)} \leq \mathbf{q} - \mathbf{T}\mathbf{u}^{*(j)} - \mathbf{H}\mathbf{y} - \mathbf{W}\boldsymbol{\delta}^{(j)} - \mathbf{S}\mathbf{z}^{(j)} - \mathbf{V}\mathbf{r}^{(j)}, \quad \forall \mathbf{u}^{*(j)} \in \mathcal{A}_{part} \quad (75)$$

$$\mathbf{Q}\mathbf{z}^{(j)} + \mathbf{F}\mathbf{r}^{(j)} \leq \mathbf{t} - \mathbf{L}\mathbf{y} - \mathbf{J}\boldsymbol{\delta}^{(j)}. \quad (76)$$

3. Solve the outer subproblem using the inner layer in the previous subsection with $\hat{\mathbf{y}}^{(j)} = \mathbf{y}^*$. Obtain an optimal solution $\mathbf{b}^T \hat{\mathbf{h}}^{(j)} + \mathbf{c}^T \mathbf{y}^*$ and an optimal attack plan $\hat{\mathbf{u}}^{(j)}$. Set $LB_{out} = \mathbf{b}^T \hat{\mathbf{h}}^{(j)} + \mathbf{c}^T \mathbf{y}^*$.
4. If $(UB_{out} - LB_{out})/UB_{out} < 10^{-5}$, $\hat{\mathbf{y}}^{(j)}$ is the optimal coupling interface and the algorithm is terminated. Otherwise, $\mathcal{A}_{part} = \mathcal{A}_{part} \cup \hat{\mathbf{u}}^{(j)}$, set $j \leftarrow j + 1$ and return to step 2.

The outputs of the algorithm are the optimal combined performance in the worst-case failure scenario and the related optimal coupling interface $\hat{\mathbf{y}}$ s.

4. Illustrative case-study

As illustrative case-study, a power network based on the IEEE 14-bus system [53] and a gas network based on the IEEE 9-bus system [54] are considered. As shown in Figure 4, the IPGNs are allocated within a 300×300 km area. The importance of each infrastructure is given by their weights, w_{PN} and w_{GN} , both equal to 0.5. Node 1 in the power network is chosen as the reference bus. Other parameter values are summarized in Appendix B. We test our model for values of K_{att} ranging from 1 to 5. We choose a representative interdependency cost-per-kilometer of 1 \$/km, for both $c_{km}^{g \leftarrow p}$ and $c_{km}^{p \leftarrow g}$. We assume budget values B_{ci} ranging from \$900 to \$1500 for the installment of coupling interfaces. We also consider a budget of \$823, which corresponds to the cost of the minimum-distance coupling interface, where each node in one infrastructure is dependent, if necessary, on the geographically-closest node of the other infrastructure⁴. We compare the results obtained by our model with the results obtained with network metrics-based coupling interfaces, which are identified based on different combinations of node degree (D) and betweenness (B). We distinguish four coupling interfaces using the different network metrics and the terms *assortative* (subscript *ast*) and *disassortative* (subscript *dst*). In network science, the assortativity (disassortativity) is a property that describes the tendency of the nodes of a network to be connected to nodes which are similar (different) regarding some specific properties [55]. For example, it can refer to the tendency of high degree nodes to be attached to other high degree nodes. Additionally, we identify a geographical location-based coupling interface, referred to as *Euclidean*. The five different network metrics-based interfaces used in this work are characterized by the following features:

- Euclidean: each node in the power network (or gas network) is dependent on the geographically closest node in the gas network (or power network).

⁴The cost of this coupling interface, referred to as *Euclidean* coupling interface, is, precisely, \$822.763752. For the sake of simplicity, in this work, it is approximated to \$823.

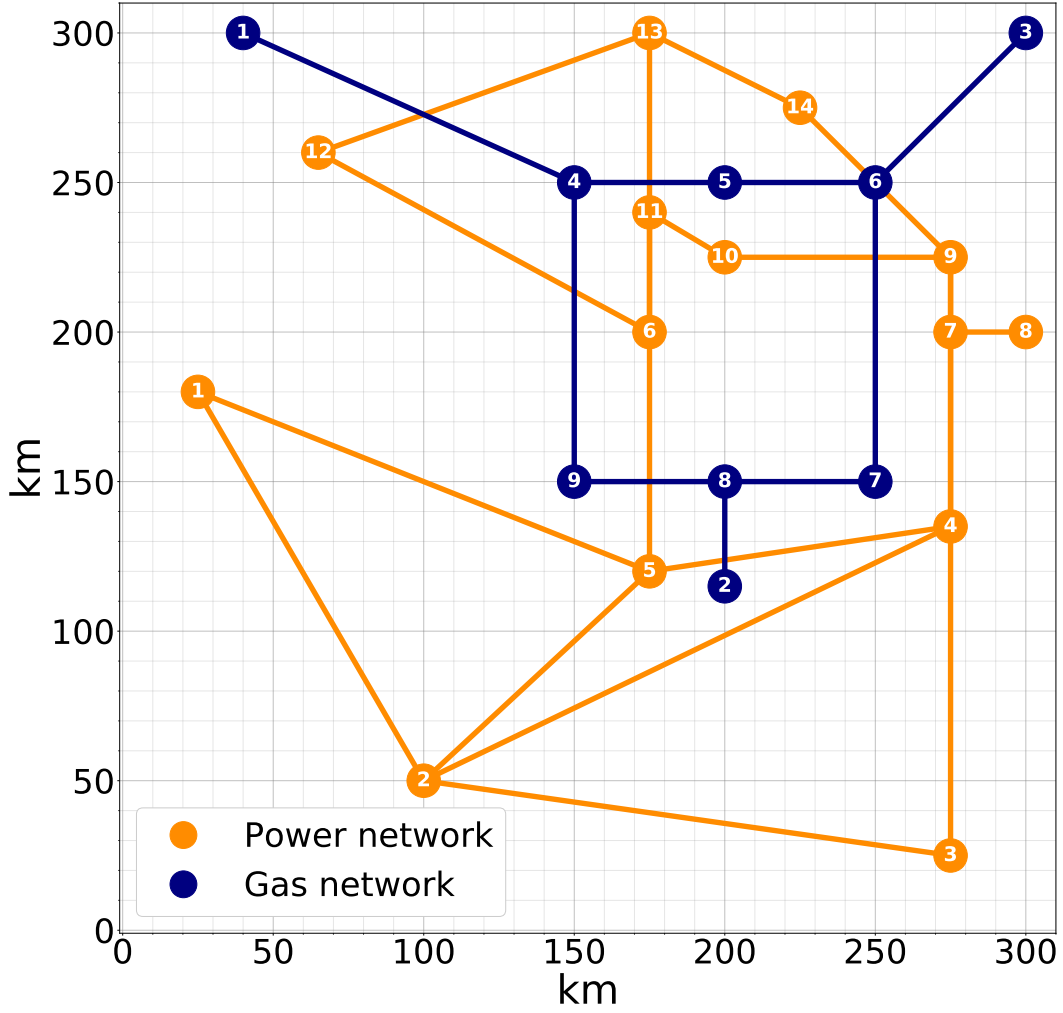


Figure 4: Interdependent power and gas networks.

- DD_{ast} : the node with the k^{th} highest degree in the power network (or gas network) is dependent on the node with the k^{th} highest degree in the gas network (or power network).
- DD_{dst} : the node with the k^{th} highest degree in the power network (or gas network) is dependent on the node with the k^{th} lowest degree in the gas network (or power network).
- BB_{ast} : the node with the k^{th} highest betweenness in the power network (or gas network) is dependent on the node with the k^{th} highest betweenness in the gas network (or power network).
- BB_{dst} : the node with the k^{th} highest betweenness in the power network (or gas network) is dependent on the node with the k^{th} lowest betweenness in the gas network (or power network).

The cost associated with each network metrics-based coupling interface is reported in Table 1.

Table 1: Cost of network metrics-based coupling interfaces. For simplicity, the costs are rounded by excess.

Interface	Cost
Euclidean	\$823
DD_{ast}	\$1518
DD_{dst}	\$2098
BB_{ast}	\$1943
BB_{dst}	\$2126

The optimization problem is implemented with Gurobi 9.1 [56] on a desktop PC with a 3.20 GHz CPU and 32 GB RAM.

5. Results and discussion

5.1. Combined performance

The results for the network metrics-based coupling interfaces are shown in Figure 5, while the results for the optimal coupling interfaces obtained by our approach with different budget B_{ci} are shown in Figure 6. The x-axis shows the maximum number of lines in the power network which can be attacked and failed; the y-axis shows the correspondent worst-case realization of the combined performance.

As it can be clearly seen in Figure 5, the DD_{ast} coupling interface performs quite poorly, reaching a worst-case combined performance value of 0 for $K_{att}=4$. The BB_{ast} coupling interface performs well for values $K_{att} \leq 4$. The DD_{dst} and BB_{dst} coupling interfaces perform similarly for values $K_{att} \leq 3$. For $K_{att}=4$, the DD_{dst} interface performs better, while for $K_{att}=5$, the BB_{dst} interface performs better.

The Euclidean coupling interface leads to the better performance overall: for $K_{att}=3$, $K_{att}=4$ and $K_{att}=5$, the Euclidean coupling interface leads worst-case combined performance of 0.703, 0.523 and 0.307. It is outperformed only by the BB_{ast} coupling interface for $K_{att}=1$.

These results clearly show how different coupling interfaces lead to different worst-case combined performance. In this case, the Euclidean coupling interface performs better than the other network metrics-based coupling interfaces. However, these results should not be generalized, as the performance of each network metrics-based coupling interface is strongly case-dependent. For example, if we change the geographical disposition of the nodes of the IPGNs, the Euclidean coupling interface would be different and, thus, the results would differ. Similar considerations are valid for the other network metrics-based coupling interfaces.

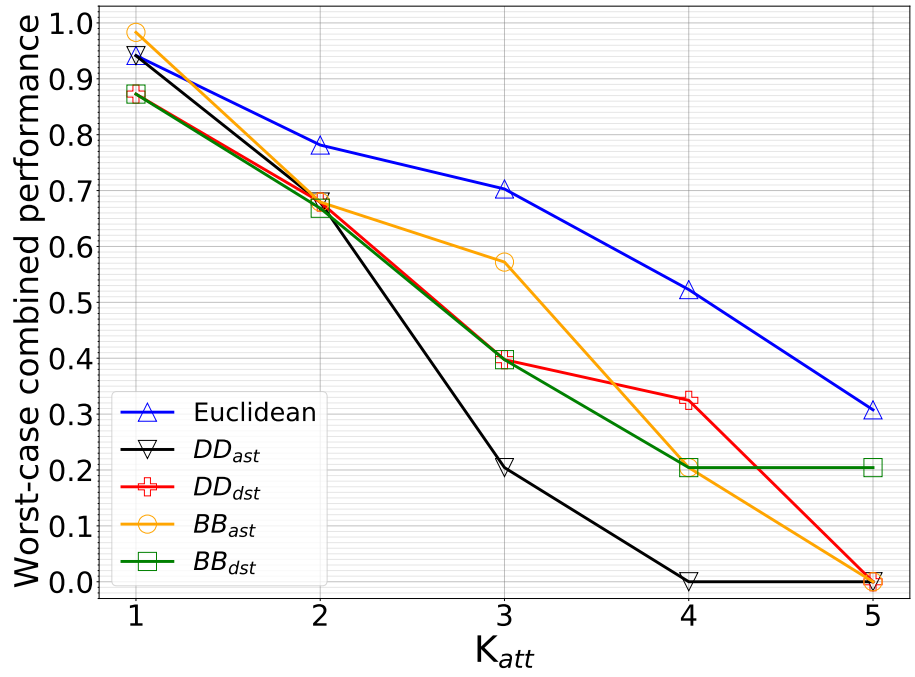


Figure 5: Worst-case combined performance for different network metrics-based coupling interface and values K_{att} .

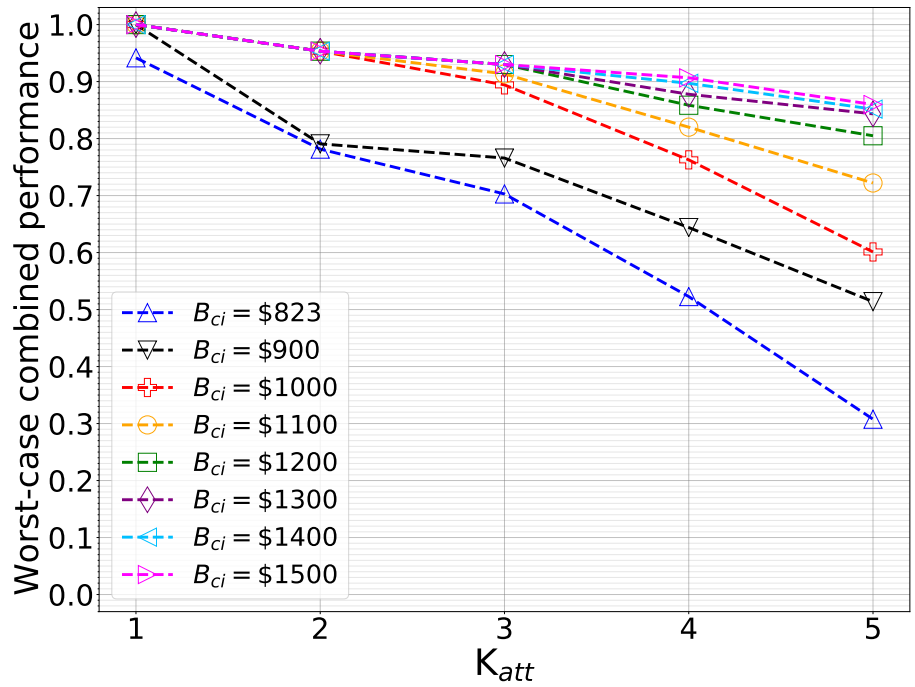


Figure 6: Worst-case combined performance for optimized coupling interface with different budgets B_{ci} and values K_{att} .

The optimal coupling interfaces, identified with the proposed optimization model, outperform the network metrics-based coupling patterns in terms of worst-case combined performance, as it can be clearly seen in Figure 6. The minimum budget which ensures the feasibility of the model is \$823, which corresponds to the cost of the Euclidean coupling interface (see Table 1). For a budget lower than \$823 it is not possible to allocate all the necessary interdependencies and to ensure satisfactory performance in normal conditions, and the optimization problem is, thus, unfeasible. The results for $B_{ci}=\$823$ (blue triangles in Figure 6) are equivalent to the results of the Euclidean coupling interface (blue triangles in Figure 5).

As it can be clearly seen, for values of B_{ci} greater than \$823, the traditional interfaces are outperformed by the optimal coupling interfaces identified by the proposed approach. For example, with $B_{ci}=\$900$ and $K_{att}=3$, $K_{att}=4$ and $K_{att}=5$, the worst-case combined performance are, respectively, 0.766, 0.644 and 0.514, while with $B_{ci}=\$1000$ and $K_{att}=3$, $K_{att}=4$ and $K_{att}=5$, the worst-case combined performance are 0.894, 0.763 and 0.601, respectively. These results are considerably higher than the previously explained Euclidean interface (0.703, 0.523 and 0.307, respectively).

The worst-case combined performance improves with the increasing of the budget B_{ci} . For example, with $B_{ci}=\$1500$ and $K_{att}=3$, $K_{att}=4$ and $K_{att}=5$, the worst-case combined performance are 0.930, 0.906 and 0.860, respectively. For values of B_{ci} greater than \$1500, the results do not improve. The case $B_{ci}=\$1500$ (pink triangles in Figure 6) leads to the best possible results for this case-study.

It is also of interest to compare optimal coupling interface designs for different B_{ci} and K_{att} . In Figure 7, the optimal coupling interfaces for $B_{ci}=\$900$ and $B_{ci}=\$1000$ with $K_{att}=2$ are shown. With $B_{ci}=\$900$ and $K_{att}=2$, the optimal value of the combined performance is 0.791, while with $B_{ci}=\$1000$ and $K_{att}=2$, the optimal value of the combined performance is 0.953. These values corresponds to an increase of combined performance of 20.5% for an increase of budget of 11.1%. As we can notice in Figure 7, two interdependency links from the gas network to the power network (red squares) change when passing from $B_{ci}=\$900$ to $B_{ci}=\$1000$, as it is also highlighted in Table 2. Moreover, three interdependency links from the power network to the gas network (blue squares) change when passing from $B_{ci}=\$900$ to $B_{ci}=\$1000$, as it is also highlighted in Table 3.

Table 2: Reallocation of interdependency links from the gas network to the power network (gas supply) when passing from $B_{ci}=\$900$ to $B_{ci}=\$1000$, with $K_{att}=2$.

Budget	Node 6 $\in V_{PN}$	Node 8 $\in V_{PN}$
\$900	Node 8 $\in V_{GN}$	Node 6 $\in V_{GN}$
\$1000	Node 9 $\in V_{GN}$	Node 7 $\in V_{GN}$

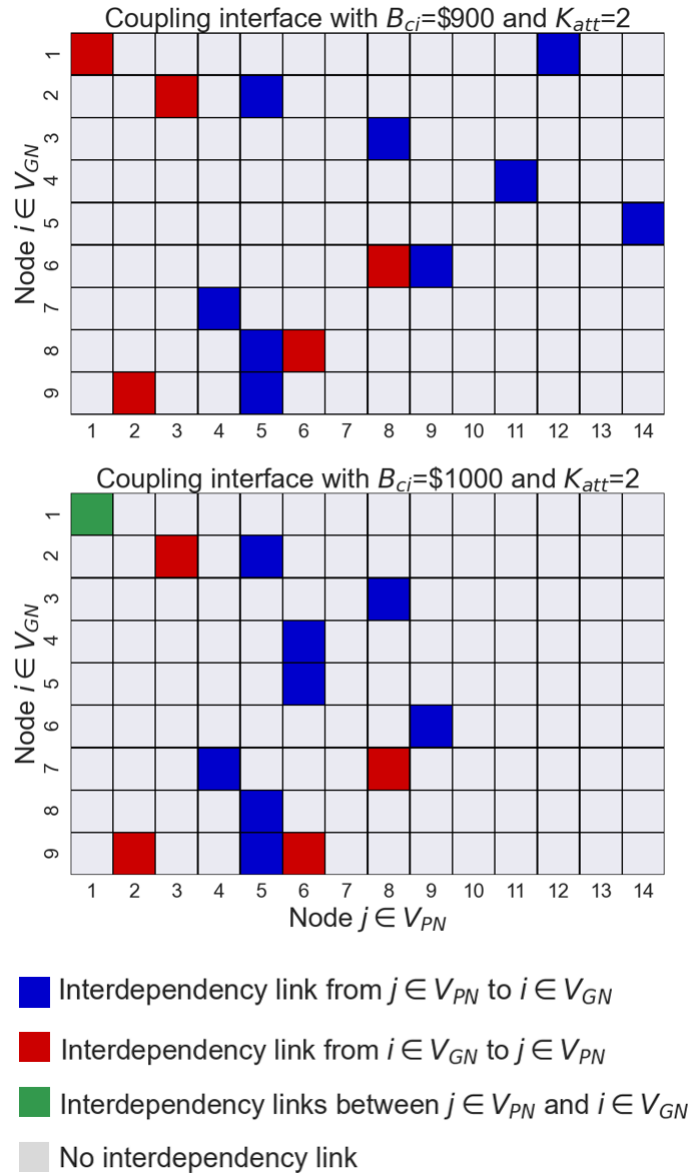


Figure 7: Example of two optimal solutions for $B_{ci}=\$900$ and $B_{ci}=\$1000$ with $K_{att}=2$. Blue squares represent links from the power network to the gas network (electricity supply); red squares represent links from the gas network to the power network (gas supply); green squares represent links in both the directions; grey squares represent the absence of links.

As it can be clearly seen, the reallocation of some of the interdependency links leads a considerable increase of worst-case combined performance. Moreover, it is interesting to notice that, with $B_{ci}=\$1000$, nodes 1, 4, and 5 of the gas network are dependent on nodes 1, 6, and 6 of the power network, respectively, and both these nodes of the power network contain a gas-fired power plant, i.e. they have some power production capacity (see Table B.5 in Appendix B). Intuitively, as in this work only failures of lines are considered, it is more convenient for nodes of the gas network to

Table 3: Reallocation of interdependency links from the power network to the gas network (electricity supply) when passing from $B_{ci}=\$900$ to $B_{ci}=\$1000$, with $K_{att}=2$.

Budget	Node 1 $\in V_{GN}$	Node 4 $\in V_{GN}$	Node 5 $\in V_{GN}$
\$900	Node 12 $\in V_{PN}$	Node 11 $\in V_{PN}$	Node 14 $\in V_{PN}$
\$1000	Node 1 $\in V_{PN}$	Node 6 $\in V_{PN}$	Node 6 $\in V_{PN}$

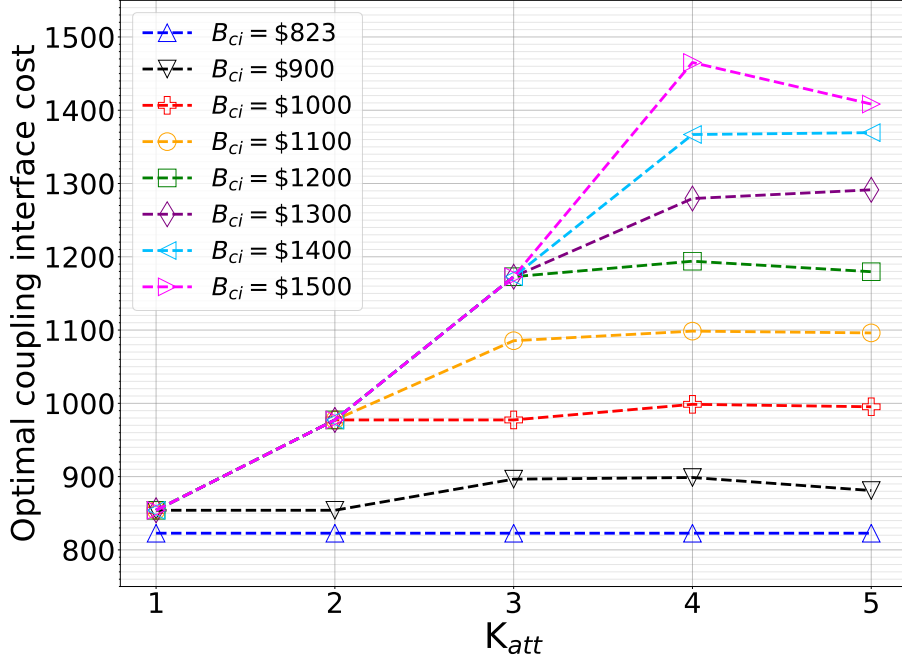


Figure 8: Cost of optimal coupling interfaces for different budgets B_{ci} and values K_{att} .

be dependent on nodes in the power network with some production capacity, and vice versa.

5.2. Coupling interface cost

In Figure 8, the results in terms of allocation cost of optimal coupling interfaces for different monetary budgets and maximum failed lines are shown. As it can be clearly seen, the network metrics-based coupling interfaces are outperformed also in terms of cost (with the exception of the Euclidean coupling interface). The cost of the network metrics-based coupling interfaces are shown in Table 1.

It is also useful to compare the increase in combined performance with the increase of cost. For example, for the case $K_{att}=3$, passing from $B_{ci}=\$823$ to $B_{ci}=\$1000$ (21.5% of budget increase) leads to an increase of 27.2% in worst-case combined performance (from 0.703 to 0.894). The cost of the optimal coupling interface with a budget $B_{ci}=\$1000$ is 977.3\$, corresponding to an increase of

cost of 18.8% from the Euclidean coupling interface. In this case, the relative increase of combined performance is greater than the relative increase of cost. However, as it can be graphically seen in Figures 6 and 8, for higher values of K_{att} and B_{ci} , the relative increase of cost is higher than the increase in performance. For example, for the case $K_{att}=5$, when passing from $B_{ci}=\$1400$ to $B_{ci}=\$1500$, the increase of budget is 7.1%, and the increase of actual cost is 2.8% (from \$1369.40 to \$1408.40); however, the increase of combined performance is only 0.93% (from 0.852 to 0.860).

For the case previously analyzed in Figure 7 and Table 3, an increase of 11.1% in the budget (from \$900 to \$1000) leads to an increase of 20.5% in combined performance (from 0.791 to 0.953). The actual costs of the two optimal solutions, for $B_{ci}=\$900$ and $B_{ci}=\$1000$ with $K_{att}=2$, are \$854.1 and \$977.3, respectively, corresponding to an increase of 14.4% in cost when passing from $B_{ci}=\$900$ to $B_{ci}=\$1000$ with $K_{att}=2$.

5.3. Validation

The last term in the objective function in (7) numerically pushes the optimization problem to identify the cheapest solution among the coupling interfaces that maximizes the combined performance of the IPGNs. In order to identify correctly this solution, the order of magnitude of the factor γ should be set properly, accounting for the order of magnitude of the combined performance, the monetary budget, and the optimality gap within the NC&CG algorithm. Within this paper, a value of $\gamma=10^{-5}$ is used. The results are then validated by solving the optimization problem only accounting for the combined performance ($\gamma=0$), and by setting the monetary budget B_{ci} slightly below the actual cost of the optimal coupling interface, and verify that the optimal combined performance are lower.

For example, for the case $B_{ci}=\$1000$ and $K_{att}=2$, the optimal coupling interface has a cost of \$977.3 and leads to combined performance of 0.953. We can verify that the cheapest optimal solution is identified correctly by setting $\gamma=0$ and solving for a budget $B_{ci}=\$977$. Solving the problem with a budget $B_{ci}=\$977$ leads to combined performance of 0.950, lower than the optimal combined performance of 0.953. This is an indication the correct cheapest optimal solution is identified correctly.

5.4. Computational performance

The computational time in seconds of the NC&CG algorithm is shown in Table 4. In this study, the computational cost is acceptable, as the longest instance of the NC&CG algorithm occurs for $B_{ci}=\$1000$ and $K_{att}=5$, and it takes 176.26 seconds.

The illustrative case-study in this work presents a small-medium size, and the computational cost might increase considerably if larger networks are considered. However, this do not represent an issue:

Table 4: Computational time in seconds of the NC&CG algorithm.

B_{ci}	$K_{att=1}$	$K_{att=2}$	$K_{att=3}$	$K_{att=4}$	$K_{att=5}$
\$823	1.13	4.12	30.17	50.37	140.30
\$900	2.91	6.26	35.58	156.44	93.36
\$1000	1.73	7.80	21.64	52.67	176.26
\$1100	2.89	11.25	22.40	21.29	47.63
\$1200	2.75	9.45	53.61	97.97	53.41
\$1300	2.87	6.31	27.94	73.95	49.66
\$1400	2.89	8.03	16.48	22.89	40.37
\$1500	2.90	5.86	12.48	39.94	42.58

- the proposed model should be used for designing or retrofitting coupling interfaces, and in preliminary design phases, the computational time do not represent a critical factor;
- the computational complexity of the optimization problem can be reduced by limiting the number of binary variables of the problem. For example, the feasible allocation of interdependency links can be limited to nodes which are geographically close to each other.

6. Conclusion

CIs are essential for any advanced society, and ensuring their resilience against failures and disruption is of the utmost importance. As coupling interfaces between interdependent CIs are a key factor for maintaining high levels of resilience, optimizing their design is an important issue.

In this work, we proposed a mathematical programming approach for the resilience-based optimization of coupling interfaces between interdependent CIs that, compared to traditional network metrics-based solutions, is more generalizable and leads to better performances.

In fact, using interdependent power and gas networks as case-study, we showed how optimal coupling strategies, obtained by the proposed approach, clearly outperform traditional coupling strategies based on network metrics. In addition, the proposed approach can be easily adapted to other combinations of interdependent CIs by updating the operational model used in the optimization procedure.

In the proposed case-study, only failures of power lines are considered. However, alternative disruption scenarios, such as failure of nodes or gas pipelines, can be easily included with a similar

approach using additional binary variables.

The computational cost is affordable in this work. In general, in this kind of optimization problems, aimed at being used during design phases, the computational time does not represent a key factor.

Further improvements of this work includes the possibility of allocating redundant interdependency links within the coupling interface and the evaluation of occurrence probability of each failure scenario.

Appendix A. Linearization of DC power flow constraint

Constraint (34) can be linearized by replacing it with the equivalent Constraints (A.1) and (A.2):

$$x_k f_k - (\theta_{O(k)} - \theta_{D(k)}) \geq -M_k(1 - u_k), \forall k \in E_{PN} \quad (\text{A.1})$$

$$x_k f_k - (\theta_{O(k)} - \theta_{D(k)}) \leq M_k(1 - u_k), \forall k \in E_{PN} \quad (\text{A.2})$$

where M_k is the “Big-M” constants, computed as in (A.3) as suggested in [50]:

$$M_k \geq \bar{\theta} + x_k \bar{f}_k \quad (\text{A.3})$$

where $\bar{\theta}$ is the maximum difference of two phase angles at two connected buses, here assumed $\pi/2$.

Appendix B. IPGNs parameters

Table B.5: Production capacity and base requested demand for each node in the power network.

Node index	\bar{p}_i [MW]	\bar{d}_i^b [MW]	$\bar{d}_i^{m^3}$ [m ³]
1	42	8.5	3
2	42	8.5	3
3	42	8.5	3
4	0	8.5	0
5	0	8.5	0
6	42	8.5	3
7	0	8.5	0
8	42	8.5	3
9	0	8.5	0
10	0	8.5	0
11	0	8.5	0
12	0	8.5	0
13	0	8.5	0
14	0	8.5	0

Table B.6: Boundaries, maximum flow capacity and reactance for each line in the power network.

Line index	Boundaries (i,j)	\bar{f}_k [MW]	x_k [pu]
1	(1, 2)	30	0.05917
2	(1, 5)	30	0.22304
3	(2, 3)	30	0.19797
4	(2, 4)	30	0.17632
5	(2, 5)	30	0.17388
6	(3, 4)	30	0.17103
7	(4, 5)	30	0.04211
8	(4, 7)	30	0.20912
9	(4, 9)	30	0.55618
10	(5, 6)	30	0.24202
11	(6, 11)	30	0.1989
12	(6, 12)	30	0.25581
13	(6, 13)	30	0.13027
14	(7, 8)	30	0.17615
15	(7, 9)	30	0.11001
16	(9, 10)	30	0.0845
17	(9, 14)	30	0.27038
18	(10, 11)	30	0.19207
19	(12, 13)	30	0.19988
20	(13, 14)	30	0.34802

Table B.7: Production capacity and base requested demand for each node in the gas network.

Node index	\bar{p}_i [m ³]	\bar{d}_i [m ³]	\bar{d}_i^{MW} [MW]
1	15	0	7
2	15	0	7
3	15	0	7
4	0	5	7
5	0	5	7
6	0	5	7
7	0	5	7
8	0	5	7
9	0	5	7

Table B.8: Boundaries and maximum flow capacity for each line in the gas network.

Line index	Boundaries (i,j)	\bar{f}_k [m ³]
1	(1, 2)	15
2	(1, 5)	10
3	(2, 3)	10
4	(2, 4)	15
5	(2, 5)	10
6	(3, 4)	10
7	(4, 5)	15
8	(4, 7)	10
9	(4, 9)	10

References

- [1] F. Nocera and P. Gardoni, "Selection of the modeling resolution of infrastructure," *Computer-Aided Civil and Infrastructure Engineering*, 2022.
- [2] A. Bellè, Z. Zeng, C. Duval, M. Sango, and A. Barros, "Modeling and vulnerability analysis of interdependent railway and power networks: Application to british test systems," *Reliability Engineering System Safety*, vol. 217, p. 108 091, 2022, ISSN: 0951-8320.
- [3] Y. Li, C. Zhang, C. Jia, X. Li, and Y. Zhu, "Joint optimization of workforce scheduling and routing for restoring a disrupted critical infrastructure," *Reliability Engineering & System Safety*, vol. 191, p. 106 551, 2019.
- [4] A. Mottahedi, F. Sereshki, M. Ataei, A. N. Qarahasanlou, and A. Barabadi, "Resilience estimation of critical infrastructure systems: Application of expert judgment," *Reliability Engineering & System Safety*, vol. 215, p. 107 849, 2021.
- [5] N. Sharma, A. Tabandeh, and P. Gardoni, "Regional resilience analysis: A multiscale approach to optimize the resilience of interdependent infrastructure," *Computer-Aided Civil and Infrastructure Engineering*, vol. 35, no. 12, pp. 1315–1330, 2020.
- [6] S. V. Buldyrev, R. Parshani, G. Paul, H. E. Stanley, and S. Havlin, "Catastrophic cascade of failures in interdependent networks," *Nature*, vol. 464, no. 7291, pp. 1025–1028, 2010.
- [7] J. Winkler, L. Dueñas-Osorio, R. Stein, and D. Subramanian, "Interface network models for complex urban infrastructure systems," *Journal of Infrastructure Systems*, vol. 17, no. 4, pp. 138–150, 2011.
- [8] M. Ouyang and L. Dueñas-Osorio, "An approach to design interface topologies across interdependent urban infrastructure systems," *Reliability Engineering & System Safety*, vol. 96, no. 11, pp. 1462–1473, 2011.
- [9] M. Ouyang, "Review on modeling and simulation of interdependent critical infrastructure systems," *Reliability engineering & System safety*, vol. 121, pp. 43–60, 2014.
- [10] G. G. Brown, W. M. Carlyle, J. Salmerón, and K. Wood, "Analyzing the vulnerability of critical infrastructure to attack and planning defenses," in *Emerging Theory, Methods, and Applications*, Informs, 2005, pp. 102–123.
- [11] T. Ding, L. Yao, and F. Li, "A multi-uncertainty-set based two-stage robust optimization to defender–attacker–defender model for power system protection," *Reliability Engineering & System Safety*, vol. 169, pp. 179–186, 2018.
- [12] W. Yuan, L. Zhao, and B. Zeng, "Optimal power grid protection through a defender–attacker–defender model," *Reliability Engineering & System Safety*, vol. 121, pp. 83–89, 2014.

- [13] N. Ghorbani-Renani, A. D. González, K. Barker, and N. Morshedlou, “Protection-interdiction-restoration: Tri-level optimization for enhancing interdependent network resilience,” *Reliability Engineering & System Safety*, vol. 199, p. 106 907, 2020.
- [14] Y.-P. Fang and E. Zio, “An adaptive robust framework for the optimization of the resilience of interdependent infrastructures under natural hazards,” *European Journal of Operational Research*, vol. 276, no. 3, pp. 1119–1136, 2019.
- [15] N. Sharma, A. Tabandeh, and P. Gardoni, “Resilience analysis: A mathematical formulation to model resilience of engineering systems,” *Sustainable and Resilient Infrastructure*, vol. 3, no. 2, pp. 49–67, 2018.
- [16] M. Panteli, P. Mancarella, D. N. Trakas, E. Kyriakides, and N. D. Hatziargyriou, “Metrics and quantification of operational and infrastructure resilience in power systems,” *IEEE Transactions on Power Systems*, vol. 32, no. 6, pp. 4732–4742, 2017.
- [17] K. S. Trivedi, V. Jindal, and S. Dharmaraja, “Stochastic modeling techniques for secure and survivable systems,” *Information assurance: Dependability and security in networked systems. Morgan Kaufmann*, pp. 171–207, 2008.
- [18] J. Johansson, H. Hassel, and A. Cedergren, “Vulnerability analysis of interdependent critical infrastructures: Case study of the swedish railway system,” *International journal of critical infrastructures*, vol. 7, no. 4, pp. 289–316, 2011.
- [19] D. Henry and J. E. Ramirez-Marquez, “Generic metrics and quantitative approaches for system resilience as a function of time,” *Reliability Engineering & System Safety*, vol. 99, pp. 114–122, 2012.
- [20] C. Poulin and M. B. Kane, “Infrastructure resilience curves: Performance measures and summary metrics,” *Reliability Engineering & System Safety*, vol. 216, p. 107 926, 2021.
- [21] Y.-P. Fang and G. Sansavini, “Optimum post-disruption restoration under uncertainty for enhancing critical infrastructure resilience,” *Reliability Engineering & System Safety*, vol. 185, pp. 1–11, 2019.
- [22] X. Liu, Y.-P. Fang, and E. Zio, “A hierarchical resilience enhancement framework for interdependent critical infrastructures,” *Reliability Engineering & System Safety*, vol. 215, p. 107 868, 2021.
- [23] M. Najarian and G. J. Lim, “Optimizing infrastructure resilience under budgetary constraint,” *Reliability Engineering & System Safety*, vol. 198, p. 106 801, 2020.

- [24] Y. Wu, Z. Chen, H. Gong, Q. Feng, Y. Chen, and H. Tang, “Defender–attacker–operator: Tri-level game-theoretic interdiction analysis of urban water distribution networks,” *Reliability Engineering & System Safety*, vol. 214, p. 107703, 2021.
- [25] J. Kong, C. Zhang, and S. P. Simonovic, “Optimizing the resilience of interdependent infrastructures to regional natural hazards with combined improvement measures,” *Reliability Engineering & System Safety*, vol. 210, p. 107538, 2021.
- [26] Y. Almoghathawi, K. Barker, and L. A. Albert, “Resilience-driven restoration model for interdependent infrastructure networks,” *Reliability Engineering & System Safety*, vol. 185, pp. 12–23, 2019.
- [27] Y. Fang and G. Sansavini, “Optimizing power system investments and resilience against attacks,” *Reliability Engineering & System Safety*, vol. 159, pp. 161–173, 2017.
- [28] J. Wu and P. Wang, “Risk-averse optimization for resilience enhancement of complex engineering systems under uncertainties,” *Reliability Engineering & System Safety*, p. 107836, 2021.
- [29] X. Zhang, H. Tu, J. Guo, *et al.*, “Braess paradox and double-loop optimization method to enhance power grid resilience,” *Reliability Engineering & System Safety*, vol. 215, p. 107913, 2021.
- [30] S. M. Rinaldi, J. P. Peerenboom, and T. K. Kelly, “Identifying, understanding, and analyzing critical infrastructure interdependencies,” *IEEE control systems magazine*, vol. 21, no. 6, pp. 11–25, 2001.
- [31] N. Sharma, F. Nocera, and P. Gardoni, “Classification and mathematical modeling of infrastructure interdependencies,” *Sustainable and Resilient Infrastructure*, vol. 6, no. 1-2, pp. 4–25, 2021.
- [32] D. D. Dudenhofer, M. R. Permann, and M. Manic, “Cims: A framework for infrastructure interdependency modeling and analysis,” in *Proceedings of the 2006 winter simulation conference*, IEEE, 2006, pp. 478–485.
- [33] R. Zimmerman, “Social implications of infrastructure network interactions,” *Journal of urban technology*, vol. 8, no. 3, pp. 97–119, 2001.
- [34] A. Bellè, Z. Zeng, M. Sango, and A. Barros, “Towards a realistic topological and functional modeling for vulnerability analysis of interdependent railway and power networks,” *Proceedings of the 31st European Safety and Reliability Conference*, pp. 2063–2070, Jan. 2021. DOI: 10.3850/978-981-18-2016-8_356-cd.

- [35] R. Parshani, S. V. Buldyrev, and S. Havlin, “Interdependent networks: Reducing the coupling strength leads to a change from a first to second order percolation transition,” *Physical review letters*, vol. 105, no. 4, p. 048 701, 2010.
- [36] G. Fu, R. Dawson, M. Khoury, and S. Bullock, “Interdependent networks: Vulnerability analysis and strategies to limit cascading failure,” *The European Physical Journal B*, vol. 87, no. 7, pp. 1–10, 2014.
- [37] O. Yagan, D. Qian, J. Zhang, and D. Cochran, “Optimal allocation of interconnecting links in cyber-physical systems: Interdependence, cascading failures, and robustness,” *IEEE Transactions on Parallel and Distributed Systems*, vol. 23, no. 9, pp. 1708–1720, 2012.
- [38] X. Wang, W. Zhou, R. Li, J. Cao, and X. Lin, “Improving robustness of interdependent networks by a new coupling strategy,” *Physica A: Statistical Mechanics and its Applications*, vol. 492, pp. 1075–1080, 2018.
- [39] S. Chattopadhyay, H. Dai, S. Hosseinalipour, *et al.*, “Designing optimal interlink patterns to maximize robustness of interdependent networks against cascading failures,” *IEEE Transactions on Communications*, vol. 65, no. 9, pp. 3847–3862, 2017.
- [40] S. Wang, L. Hong, and X. Chen, “Vulnerability analysis of interdependent infrastructure systems: A methodological framework,” *Physica A: Statistical Mechanics and its applications*, vol. 391, no. 11, pp. 3323–3335, 2012.
- [41] H. Guo, S. S. Yu, H. H. Iu, T. Fernando, and C. Zheng, “A complex network theory analytical approach to power system cascading failure—from a cyber-physical perspective,” *Chaos: An Interdisciplinary Journal of Nonlinear Science*, vol. 29, no. 5, p. 053 111, 2019.
- [42] Z. Chen, J. Wu, Y. Xia, and X. Zhang, “Robustness of interdependent power grids and communication networks: A complex network perspective,” *IEEE Transactions on Circuits and Systems II: Express Briefs*, vol. 65, no. 1, pp. 115–119, 2017.
- [43] D. F. Rueda and E. Calle, “Using interdependency matrices to mitigate targeted attacks on interdependent networks: A case study involving a power grid and backbone telecommunications networks,” *International Journal of Critical Infrastructure Protection*, vol. 16, pp. 3–12, 2017.
- [44] N. Sharma and P. Gardoni, “Mathematical modeling of interdependent infrastructure: An object-oriented approach for generalized network-system analysis,” *Reliability Engineering & System Safety*, vol. 217, p. 108 042, 2022.

- [45] S. G. Nurre, B. Cavdaroglu, J. E. Mitchell, T. C. Sharkey, and W. A. Wallace, “Restoring infrastructure systems: An integrated network design and scheduling (inds) problem,” *European journal of operational research*, vol. 223, no. 3, pp. 794–806, 2012.
- [46] M. Ouyang and Y. Fang, “A mathematical framework to optimize critical infrastructure resilience against intentional attacks,” *Computer-Aided Civil and Infrastructure Engineering*, vol. 32, no. 11, pp. 909–929, 2017.
- [47] A. D. González, L. Dueñas-Osorio, M. Sánchez-Silva, and A. L. Medaglia, “The interdependent network design problem for optimal infrastructure system restoration,” *Computer-Aided Civil and Infrastructure Engineering*, vol. 31, no. 5, pp. 334–350, 2016.
- [48] M. Ouyang, “A mathematical framework to optimize resilience of interdependent critical infrastructure systems under spatially localized attacks,” *European Journal of Operational Research*, vol. 262, no. 3, pp. 1072–1084, 2017.
- [49] Y.-P. Fang, G. Sansavini, and E. Zio, “An optimization-based framework for the identification of vulnerabilities in electric power grids exposed to natural hazards,” *Risk Analysis*, vol. 39, no. 9, pp. 1949–1969, 2019.
- [50] L. Zhao and B. Zeng, “Vulnerability analysis of power grids with line switching,” *IEEE Transactions on Power Systems*, vol. 28, no. 3, pp. 2727–2736, 2013.
- [51] B. Zeng and L. Zhao, “Solving two-stage robust optimization problems using a column-and-constraint generation method,” *Operations Research Letters*, vol. 41, no. 5, pp. 457–461, 2013.
- [52] L. Zhao and B. Zeng, “An exact algorithm for two-stage robust optimization with mixed integer recourse problems,” *submitted, available on Optimization-Online. org*, 2012.
- [53] Accessed: 30/03/2022. [Online]. Available: <https://icseg.iti.illinois.edu/ieee-14-bus-system/>.
- [54] Accessed: 30/03/2022. [Online]. Available: <https://icseg.iti.illinois.edu/wsc-9-bus-system/>.
- [55] M. E. Newman, “Mixing patterns in networks,” *Physical review E*, vol. 67, no. 2, p. 026 126, 2003.
- [56] L. Gurobi Optimization, *Gurobi optimizer reference manual*, 2021. [Online]. Available: <http://www.gurobi.com>.